and the left-circularly polarized echo was received by both sites. The signal was phase reversal–modulated by means of a 31-element 500-μsec code (*1*). The received signals were decoded, and their frequencies were analyzed with 1-hz resolution. This separates the planetary surface into "range rings" and "Doppler strips." The resolution varies with the size of the "range-Doppler cell," which is at best about 150 km square on the planet's surface and becomes elongated toward the "Doppler equator" (a line perpendicular to the apparent rotation axis going through the subradar point). The signals from the two sites are then cross-multiplied to obtain the complex cross power or "fringe amplitude and phase" for each range-Doppler cell. The fringe pattern is rotated so that lines of constant phase are normal to the axis of apparent rotation of the planet. Thus two cells with the same range and Doppler shift contribute to the complex cross power with phases that are equal in magnitude and opposite in sign. The fringe spacing along the apparent rotation axis is due to the projection of the base line onto the axis. Typically, this amounted to about six fringes across the planet's disk.

If the fringe phase of the upper cell of an ambiguous pair is ϕ, the sum of the powers from the two cells is

$$P_u + P_l = \text{(real part of cross power)}/\cos\phi \quad (1)$$

and the difference of powers is

$$P_u - P_l = \text{(imaginary part of cross power)}/\sin\phi \quad (2)$$

These equations are solved for P_u and P_l by least-squares analysis for a set of observations over which ϕ varies considerably because of variation in the projected base line.

To correct for the drifting of the fringe pattern owing to irregularities of refraction in the earth's atmosphere, the echo from the subradar region was used as a "phase calibrator" every 15 seconds; that is, the fringe phase of the subradar region was measured and all other phases were referred to it. The effects of the Venus atmosphere on the location of the range-Doppler cells should be negligible on the scale of resolution observed for a model based on a CO_2 atmosphere with a pressure of 200 atm at the surface. Effects become serious near the limb but the map does extend far enough back to require correction.

Figure 1 maps the radar reflectivity on a system of planetary coordinates defined by Carpenter (*2*). The intensities have been scaled to take into account the "mean planetary scattering law" so that the intensity represents the fraction of the mean planetary scattering appropriate for that distance from the subradar region. Thus a uniformly rough planet (made of a homogeneous material) would appear uniformly bright if we assume that backscatter results from roughness. A perfectly smooth planet produces only a specular reflection at the subradar point.

The map was produced by averaging periods of observation, each about 7 hours long, made over 5 days at the time of inferior conjunction this year. The data were processed and displayed by a digital computer. Coordinate transformation was performed on the assumption that the planet rotated in a retrograde fashion with the earth synchronous period of 243.16 days. The axis direction (*4*) was assumed to have a right ascension of 270.3° and a declination of 66.7°.

The map's extent is limited by code length and a bandwidth of 64.5 hz (which is less than the Doppler spread across the planet). Fine structure toward the edges of the map is mainly noise. The strong feature at −26° latitude and 0° longitude has a signal-to-noise ratio of about 20 standard deviations. The signal-to-noise ratio of the map improves closer to the subradar region. Generally, noise can be recognized by its lack of correlation from cell to cell.

Figure 2 shows a diagram of the features taken from the intensity map and identifies them with features located by Carpenter (*2*) and those observed by means of the Haystack-Westford antennas (*4*) at the last conjunction. New features are labeled by their central coordinates—longitude in degrees followed by latitude in degrees. The map shows dark circular features (two of the most prominent are labeled 312-14 and 335-28) not seen in previous data probably because of the poor signal-to-noise ratios obtained in previous maps. These circular features have the size and appearance of lunar maria although any physical similarity is mere speculation at this stage.

A. E. E. Rogers
R. P. Ingalls
Lincoln Laboratory, Massachusetts Institute of Technology, Lexington 02173

References and Notes

1. J. V. Evans and T. Hagfors, Eds., *Radar Astronomy* (McGraw-Hill, New York, 1968).
2. R. L. Carpenter, *Astron. J.* **71**, 142 (1966).
3. A. E. E. Rogers, T. Hagfors, R. A. Brockelman, R. P. Ingalls, J. I. Levine, G. H. Pettengill, F. S. Weinstein, *M.I.T. Lincoln Lab. Tech. Rep. 444* (1968); R. P. Ingalls, R. A. Brockelman, J. V. Evans, J. I. Levine, G. H. Pettengill, L. P. Rainville, A. E. E. Rogers, F. S. Weinstein, *M.I.T. Lincoln Lab. Tech. Rep. 456* (1968).
4. R. B. Dyce, G. H. Pettengill, I. I. Shapiro, *Astron. J.* **72**, 351 (1967).
5. We are grateful to the entire staff of the Haystack Research Facility and the Westford Communications Terminal, particularly J. Butterworth, P. Okerholm, and J. Sobolewski for their technical assistance, and P. B. Sebring, B. E. Nichols, and H. H. Hoover for their enthusiasm in helping to organize the project. We also thank M. E. Ash, I. I. Shapiro, and W. B. Smith for the ephemeris computations and gratefully acknowledge the work of T. Hagfors, R. A. Brockelman, G. H. Pettengill, and J. I. Levine in the original concept and design of the radar interferometer. Sponsored by the U.S. Air Force.

13 May 1969

Carbonado: Natural Polycrystalline Diamond

Abstract. *Carbonados are porous aggregates of mostly xenomorphic diamond crystallites ranging in diameter from a fraction of a micron to over 20 microns. Crystalline inclusions (up to 3 percent) occur in the pores of the crystallites and consist mainly of orthoclase and small amounts of other igneous, metamorphic, and secondary minerals.*

The term "carbonado" (black diamond) was originally coined by Brazilian miners to designate the opaque, black or gray, polycrystalline diamond found mainly in the highlands of Bahia, Brazil, and in smaller amounts in Venezuela and British Guiana. Carbonado makes up only 0.1 percent of the world's production of industrial diamonds, but, because of its extraordinary toughness, it is often used in combination with bort diamonds as studding on drill bits designed to pierce hard rocks.

Carbonado has been known as a distinct form of diamond since at least 1843. Roth *et al.* (*1*) and Gerlach (*2*) postulated the presence of amorphous carbon or graphite as a coloring and binding agent between diamond crystallites. Brandenberger (*3*) found no such evidence in x-ray diffraction diagrams and assumed that carbonados are masses of crystallites resembling the aggregates of crystals found in metals. Fettke and Sturgis (*4*) and Kerr *et al.* (*5*) examined carbonados by light microscopy and observed the existence of

Table 1. Mineral inclusions in carbonado diamond identified by x-ray diffraction.

Elements associated in inclusions*	Corresponding minerals
Si, Al, K	Orthoclase, $KAlSi_3O_8$
Fe (Cr)	Hematite + goethite, $Fe_2O_3 + FeO(OH)$
Si, Al, Ca (Mg)	Gehlenite, $Ca_2Al_2SiO_2{\cdot}H_2O$
Si, Al, Ca, Fe, Ce (Pr, Nd)	Allanite, $(Ca,Fe)_2(Al,Ce\ Fe)_3Si_3O_{12}(OH)$
Ca, Ti	Perovskite, $CaTiO_3$
Si, Zr (Hf)	Zircon, $ZrSiO_4$
Ti, Al	Rutile + corundum, $TiO_2 + Al_2O_3$
Sn	Cassiterite, SnO_2
Si, Al, Fe	Chloritoid, $FeAl_2SiO_5(OH)_2$
Cu, P	Pseudomalachite, $Cu_5(PO_4)_2(OH)_4$
Cu, S	Covellite, CuS
Cu, Zn	Rosasite, $(Cu,Zn)_2CO_3(OH)_2$
Ca, Ce (La)	Parisite, $2\ CeFCO_3{-}CaCO_3$
Ca, S	Anhydrite, $CaSO_4$

* Elements in parentheses are present as traces.

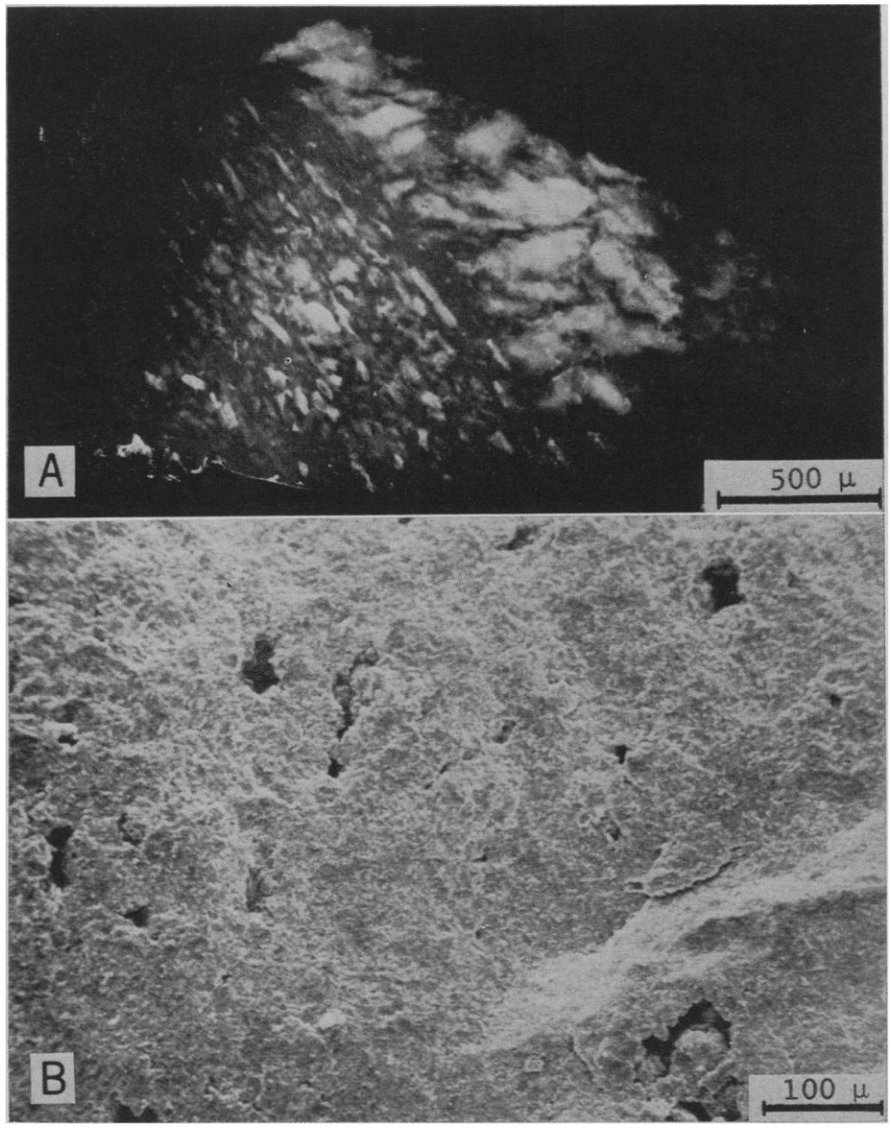

Fig. 1. (A) Radiograph (negative print) of carbonado showing silicate inclusions; (B) scanning electron micrograph of fractured carbonado surface.

crystallites between 20 and 95 μ in diameter. These authors also attributed the dark gray color of the stones to the presence of various metallic oxides and minerals and either amorphous carbon or graphite.

Some insight into the conditions of formation of carbonado can be gained from the diamond-synthesis work of Wentorf and Bovenkerk (*6*), who found that, under conditions of pressure and temperature substantially above the univariant pressure-temperature equilibrium curve between diamond and graphite, the nucleation rate of diamond is very high. This rate of nucleation results in the growth of large numbers of small and imperfect diamonds aggregated into black lumps. Carbonado might thus form under the effect of rapid cooling-off processes at high pressures, or by a sudden increase in pressure at moderately high temperatures in a suitable plutonic geochemical environment.

The meteoritic and explosively shock-synthesized varieties of polycrystalline diamond have been investigated in recent years (*7*) whereas natural carbonado has received very little attention despite its industrial applications. We undertook a detailed characterization of carbonado by a combination of light, electron, and scanning electron microscopy with electron-probe microanalysis and x-ray diffraction.

About 50 carbonados, each weighing up to 0.6 carat, were obtained from the Sincorá–Morro do Chapéu area in the state of Bahia, Brazil. According to a survey by Branner (*8*), the geology of the region with which the carbonados are associated consists of folded and faulted sediments overlying extensive serpentinized peridotites from which originate basic igneous dikes traversing the overlying deposits. The sediments consist of Devonian Caboclo shales, Carboniferous pink Lavras quartzites, conglomerate, and sandstones overlain by Triassic red Estancia sandstones covered by Jurassic Salite limestones. The carbonados appear to be most closely related to the Lavras series which dominates the topographic heights and from which most diamond-bearing streams originate. To the east of these sedimentary deposits are extensive deposits of crystalline rocks consisting of Precambrian schists, gneisses, granites, and various other eruptive and metamorphic rocks.

Under reflected light the carbonado

specimens had a dark-gray metallic luster; fractured surfaces were of a lighter gray. Examination with a light microscope showed a highly variable number of pores which result in densities ranging from 3.326 to 3.434 g cm^{-3}; this is substantially below the density of pure-white monocrystalline diamond, namely, 3.511 g cm^{-3}. Bulk densities, that is, including open pores as determined from wax-coated specimens, varied from 3.101 to 3.392 g cm^{-3}; this shows that a significant fraction of the pores was open. These pores are irregularly shaped, usually elongated holes ranging from 10 to over 100 μ in diameter (Fig. 1B). and they often contain yellowish, white, or pink crystalline inclusions which are mainly silicates.

We determined the size and distribution of diamond crystallites in carbonados from fractured surfaces by scanning electron microscopy and electron microscopy of replicas. In most samples the crystallite size varied between 0.5 and 20 μ in diameter, with a flat maximum of the distribution curve between 1 and 4 μ.

Figure 2 shows that the crystallites generally have distorted octahedral shapes and are interlocked; interstices between larger particles are often filled with small, sometimes well-formed, diamond {111} crystallites, as seen in Fig. 2. Fracture was mainly transgranular; the smooth surfaces (Fig. 2) are octahedral planes where easy cleavage occurs. This dominant tendency of the carbonados to exhibit the {111} form is quite in accord with expectations based on the application of the Donnay-Harker principle to the diamond $Fd3m$ space group and indicates that no significant structural distortion exists within the diamond crystals. Intergranular fracture was occasionally observed; such surfaces often exhibited pores 500 Å wide which are presumed to be gas bubbles trapped along crystallite boundaries during the formation of the carbonados. Preferred orientation of the diamond crystallites was found in a significant number of micrographs. This evidence and the fact that the pores are often elongated and aligned, as shown in Fig. 1, indicate a directional flow of the carbonados in the magma or some other type of directional pressure gradient.

Fragments extracted with the replicas occasionally had edges that were sufficiently thin for electron transmission at 100 kv. Selected area electron diffraction confirmed that these particles were monocrystalline diamonds. Examination at high magnification revealed a few dislocations and straight grain boundaries without any evidence of foreign phases or of a cementing medium for the diamond crystallites.

In monocrystalline diamonds, inclusions occur within the crystals; in car-

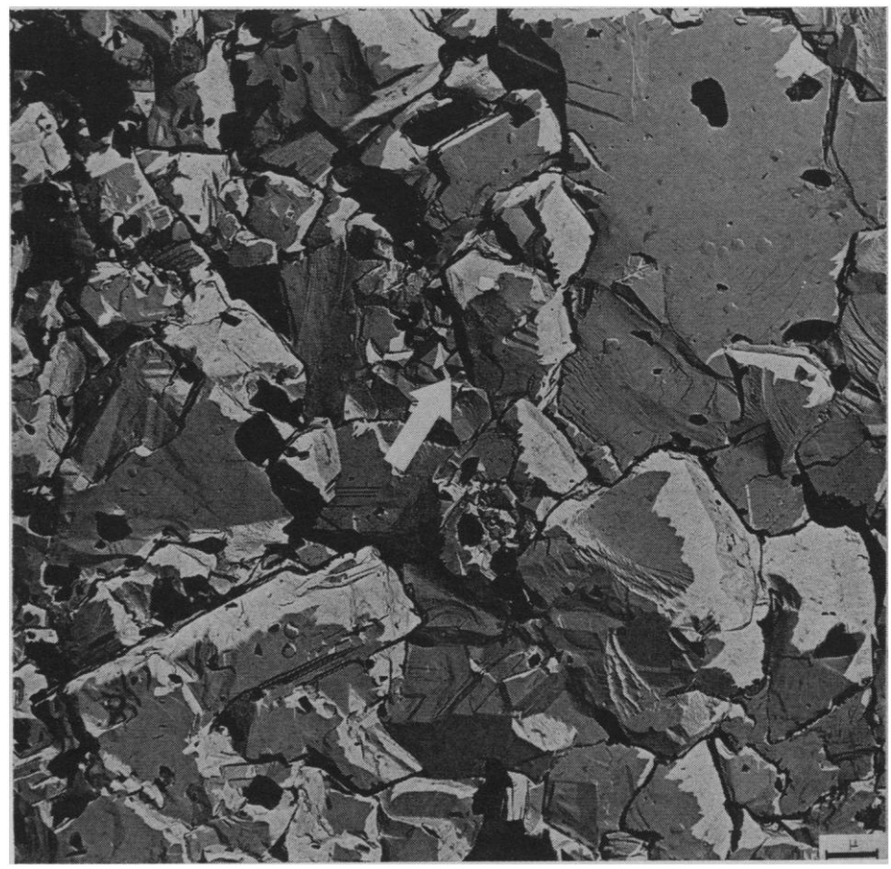

Fig. 2 (right). Replica of an electron micrograph of fractured carbonado surface. The arrow points to a near-perfect octahedron 0.5 μ in diameter.

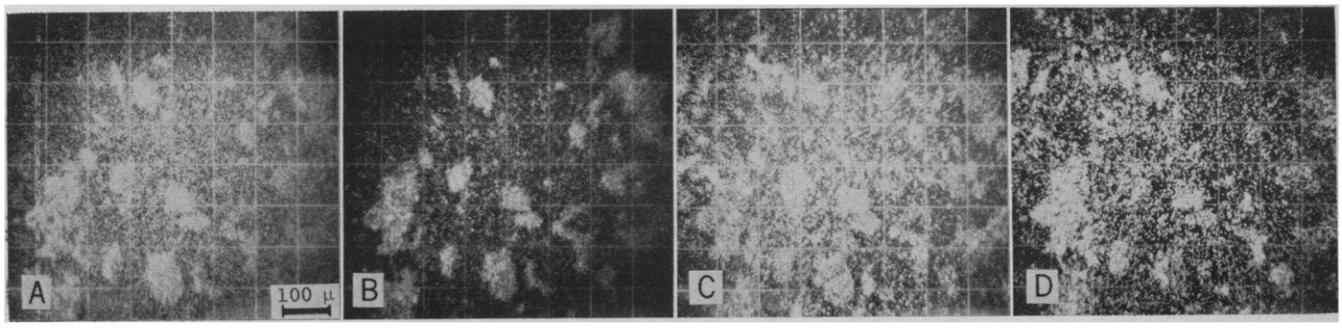

Fig. 3 (below). X-ray area scans (Kα radiation) of polished carbonado surface showing inclusions with the predominant elements aluminum (A), silicon (B), potassium (C), and iron (D). X-ray powder diffraction diagrams showed that these elements are present as orthoclase and hematite.

bonado, however, variable amounts of mineral inclusions fill part of the pores and no evidence was found of inclusions within the crystallites themselves. Examination of the outer surfaces and fractured surfaces of carbonados yields only limited information on the number and location of these inclusions whose size and distribution were obtained by contact radiography with high-resolution plates. The number of inclusions varied greatly from sample to sample, but the stone shown in Fig. 1A is a representative example. Electron-probe microanalysis showed that the most frequently encountered type of inclusion contained the elements silicon, aluminum, potassium, and iron. Minor amounts of phosphorus, sulfur, calcium, titanium, copper, zinc, zirconium, tin, and cerium as well as traces of magnesium, lanthanum, praseodymium, neodymium, and hafnium were also detected. The distribution of the most frequent elements was mapped by means of x-ray area scans such as the ones shown in Fig. 3. The combinations in which the elements occur were determined from goniometer scans over a large number of discrete spots 2 to 3 μ in diameter (Table 1).

Several carbonados were heated in a quartz boat to 800°C in order to burn away the diamond. The residue (3 percent) was a pale-yellow powder; its x-ray diffraction diagram revealed only monazite, rutile, and hematite, but analysis by x-ray fluorescence confirmed the elements listed in Table 1. The heat evolved by the combustion of the diamonds apparently caused melting of all the silicates and the formation of glasses and cerium phosphate; only rutile and hematite were unchanged.

Aside from strong diamond *hkl* lines, powder x-ray diagrams of crushed carbonado contained a considerable number of weak nondiamond lines, caused by a complex mixture of minerals, the identification of which was considerably facilitated by the microprobe data. These minerals are listed in Table 1; most of them are silicates with minor amounts of phosphates, carbonates, titanates, oxides, and sulfides. It was estimated that at least 80 percent of the inclusions are composed of orthoclase, often in association with hematite. With the exception of chloritoid, which is metamorphic, most of the minerals listed in Table 1 are either primary or common accessory constituents of igneous rocks which are normally associated with diamond. Pseudomalachite, covellite, anhydrite, rosasite, and parisite are secondary minerals of hydrothermal origin.

Assumptions concerning the geochemical history of carbonado may thus be made on the basis of the mineral inclusions it contains in easily detectable amounts. For example, the presence of minerals such as allanite and corundum are indicative of a deep-seated igneous origin, and chloritoid is regarded as an indication of the dynamic metamorphism of rocks. A secondary ore such as covellite results from an enrichment process related to a descending solution. It may thus be assumed that the carbonados were originally formed in basic magmatic rocks that were later subjected to metamorphic and erosional processes resulting in eventual detrital deposits. The relatively low percentage of ultrabasic mineral inclusions in carbonado is indicative of long exposure to an erosional environment. The unusual combination of orthoclase, an acidic igneous mineral, with more basic minerals such as gehlenite could indicate that an initial basic mineral containing gehlenite intruded into granitic rock mass rich in orthoclase. In certain instances, however, a mellilite such as gehlenite is represented in a high-temperature low-pressure sanidinite metamorphic facies. Therefore the gehlenite could also have formed by contact metamorphosis of existing rock debris with intruding diamond-bearing magma. Such an interpretation is in agreement with the geological conditions at the site of carbonado deposits.

LUCIEN F. TRUEB
E. CHRISTIAAN DE WYS
Metallurgy Division, Denver Research Institute, University of Denver, Denver, Colorado 80210

References and Notes

1. W. A. Roth, G. Naeser, O. Dopke, *Chem. Ber.* **59**, 1397 (1926).
2. W. Gerlach, *Z. Anorg. Chem.* **137**, 331 (1924).
3. E. Brandenberger, *Schweiz. Mineral. Petrogr. Mitt.* **10**, 490 (1930).
4. C. R. Fettke and F. C. Sturgis, *Amer. Mineral.* **18**, 172 (1933).
5. P. F. Kerr, D. L. Graf, S. H. Ball, *ibid.* **33**, 251 (1948).
6. R. N. Wentorf and H. P. Bovenkerk, *Astrophys. J.* **134**, 995 (1961).
7. M. E. Lipschutz and E. Anders, *Science* **134**, 2095 (19[illegible] M. E. Lipschutz, *ibid.* **138**, 1266 (19[illegible] *ibid.* **143**, 1431 (1964); L. F. Trueb, *J. Appl. Phys.* **39**, 4707 (1968).
8. J. C. Branner, *Eng. Mining J.* **87**, 981 (1909).
9. One of us (L.F.T.) thanks the Explosives Department of E. I. du Pont de Nemours & Co., Eastern Laboratory, Gibbstown, N.J., for the carbonado samples and support of this work during his association with the company.

6 January 1969; revised 3 June 1969

Microphotometric Determination of Preferred Orientation in Undeformed Dolomites

Abstract. *Preferred orientation was observed in certain undeformed dolomites with a microphotometric technique. The preferred direction of the* c*-axis was found to be perpendicular to the bedding planes. The degree of orientation is rather slight, but is considered significant due to the fact that thousands of crystals are included in each measurement. It is suggested that the preferred orientation was acquired during an early diagenetic stage of dolomitization, when the individual crystals could rotate and adjust their position so that their maximum cross section tended to lie horizontally.*

Petrofabric analysis of no more than 45 limestones and dolomites have been reported (*1*). The results of these studies, summed up by Johnson (*1*) as "isotropism is the rule, anisotropism the exception," and the tedious work involved in carrying out a conventional petrofabric analysis discouraged further research on the subject.

Microphotometric techniques which were introduced in recent years as an aid to the petrofabric studies of sandstones, lavas, and shales (*2–4*) are simple and reliable. The advantage of this method lies in the fact that the orientation of many thousands of crystals (depending on the crystal size and the field diameter) is readily integrated to give a meaningful result. In this way, the time element involved in carrying out the measurements and computing the results is reduced to a minimum, and the significance of the analysis is increased. The microphotometric method is therefore an ideal tool for detecting preferred orientation in rocks whose fabric is only slightly organized and which are not considered appropriate for conventional petrofabric analysis.

I checked for anisotropism 74 thin sections of various dolomites taken from an Upper Cretaceous section in northern Israel. Some of the rocks are thinly bedded to laminar, and their mosaic is composed of anhedral to subhedral crystals, 2 to 150 μ in size. The rocks were examined in sections cut perpendicular or parallel to the bedding planes.

The light-sensing equipment used in my study consists of a photoconductive cell, a stabilized d-c variable voltage source (up to 100 volts), and a milli-